Research article

Behnood G. Ghamsari*, Anthony Olivieri, Fabio Variola and Pierre Berini

Enhanced Raman scattering in graphene by plasmonic resonant Stokes emission

Abstract: Exploiting surface plasmon polaritons to enhance interactions between graphene and light has recently attracted much interest. In particular, nonlinear optical processes in graphene can be dramatically enhanced and controlled by plasmonic nanostructures. This work demonstrates Raman scattering enhancement in graphene based on plasmonic resonant enhancement of the Stokes emission, and compares this mechanism with the conventional Raman enhancement by resonant pump absorption. Arrays of optical nanoantennas with different resonant frequency are utilized to independently identify the effects of each mechanism on Raman scattering in graphene via the measured enhancement factor and its spectral linewidth. We demonstrate that, while both mechanisms offer large enhancement factors (scattering cross-section gains of 160 and 20 for individual nanoantennas, respectively), they affect the graphene Raman spectrum quite differently. Our results provide a benchmark to assess and quantify the role and merit of each mechanism in surface-plasmon-mediated Raman scattering in graphene, and may be employed for design and realization of a variety of graphene optoelectronic devices involving nonlinear optical processes.

***Corresponding author: Behnood G. Ghamsari,** School of Electrical Engineering and Computer Science, University of Ottawa, 800 King Edward Ave., Ottawa, ON, K1N 6N5, Canada; and Centre for Research in Photonics at the University of Ottawa, 800 King Edward Ave., Ottawa, ON, K1N 6N5, Canada, e-mail: ghamsari@uottawa.ca
Anthony Olivieri: School of Electrical Engineering and Computer Science, University of Ottawa, 800 King Edward Ave., Ottawa, ON, K1N 6N5, Canada; and Centre for Research in Photonics at the University of Ottawa, 800 King Edward Ave., Ottawa, ON, K1N 6N5, Canada
Fabio Variola: Department of Mechanical Engineering, University of Ottawa, 161 Louis Pasteur St., Ottawa, ON, K1N 6N5, Canada; and Department of Physics, University of Ottawa, 150 Louis Pasteur St., Ottawa, ON, K1N 6N5, Canada
Pierre Berini: School of Electrical Engineering and Computer Science, University of Ottawa, 800 King Edward Ave., Ottawa, ON, K1N 6N5, Canada; Department of Physics, University of Ottawa, 150 Louis Pasteur St., Ottawa, ON, K1N 6N5, Canada; and Centre for Research in Photonics at the University of Ottawa, 800 King Edward Ave., Ottawa, ON, K1N 6N5, Canada

Edited by Volker Sorger

Keywords: optical nanoantennas; graphene; plasmonics; Raman scattering.

DOI 10.1515/nanoph-2014-0014
Received July 14, 2014; accepted October 5, 2014

1 Introduction

Graphene exhibits remarkable potential for nanophotonics and optoelectronic devices [1, 2]. The fast carrier dynamics and high mobility in graphene promise ultrafast devices and its wide-band interaction with light presents a viable platform for optoelectronics from the far-infrared part of the spectrum up to the visible regime. Moreover, physical properties of graphene, such as its Fermi level, may be widely tuned by means of an external electrostatic field, which is of great importance for device applications. The interaction of light with graphene can be efficiently enhanced and controlled by means of plasmonic nanostructures. Therefore, the integration of graphene with surface plasmon polariton (SPP) structures has recently attracted much interest [3–7]. In particular, nonlinear optical processes can be significantly enhanced in graphene due to the SPP resonance associated with metal nanostructures. Raman scattering exemplifies one such nonlinear phenomenon that not only has significant applications in sensing and spectroscopy, but also provides an excellent tool to study SPP-mediated nonlinear optical processes in graphene.

Plasmonic structures, in general, can enhance nonlinear optical processes, including Raman scattering, through two direct mechanisms: first by enhancing the local incident field due to the resonant SPP absorption at the pump wavelength; and second by enhancing the emission rate due to the increased density of optical states at the scattered wavelength [8–10]. If the incident and scattered wavelengths significantly differ, e.g., in the second/third harmonic generation, clearly only one of the mechanisms is supported by the SPP resonant mode. However,

for Raman scattering, where the pump and Stokes wavelengths are relatively close, both mechanisms could simultaneously contribute to the enhancement [11, 12]. Graphene possesses at least three well-separated Raman scattering peaks, namely the D, G, and 2D peaks, corresponding to a relative red-shift equivalent to approximately 1350, 1570, and 2700 cm^{-1}, respectively. For instance, at an incident wavelength of 633 nm, the associated Stokes wavelengths are equal to 692, 703, and 763 nm, respectively [13–15].

The effectiveness of plasmonic nanostructures to enhance Raman scattering in graphene has been recently demonstrated by utilizing metal nanoparticles and patterned nanostructures on or in close proximity of a graphene sheet [16–24]. While reports of large Raman enhancement factors are abundant in the literature, nonetheless, little work has been done on distinguishing resonant pump absorption from resonant Stokes emission and investigating the peculiar effects of each individual mechanism on the Raman spectrum of graphene. This deficiency is partly because realizing Raman enhancement purely based on only one mechanism is difficult due to the broad SPP resonance of the mediating plasmonic nanostructures. For instance, metal nanoparticles, often used for surface-enhanced Raman spectroscopy, possess broad Mie resonance that covers both the laser line as well as the Stokes wavelengths. In such cases both mechanisms usually contribute to the Raman enhancement and are referred to, in aggregate, as the *electromagnetic* mechanism in contrast to the *chemical* mechanism [25].

In this work we have fabricated arrays of gold monopole nanoantennas on monolayer graphene with sufficiently high quality factors in order to demonstrate Raman enhancement *exclusively* based on resonant Stokes emission or resonant pump absorption. Here, scanning Raman microscopy (See Materials and methods) is used to measure the enhancement of G and 2D peaks as a result of coupling to the nanoantennas of different lengths and widths, i.e., different resonant wavelengths, as shown in

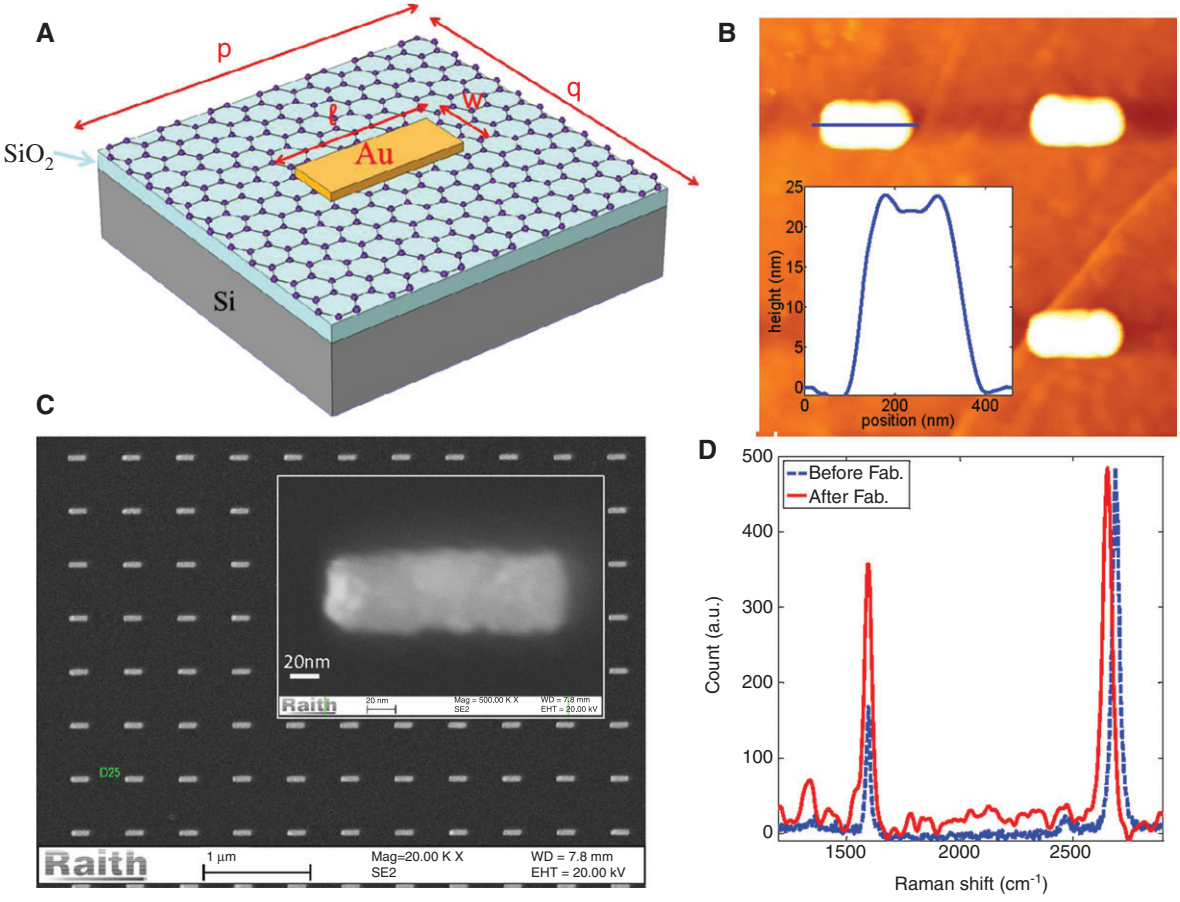

Figure 1 (A) Schematic of the unit cell of the monopole nanoantenna arrays. (B) AFM profile of a single nanoantenna. The inset depicts the line cut along the blue line in the image. (C) SEM image of a typical nanoantenna array (173 nm-long). The inset shows an individual nanoantenna. (D) Raman spectra on the graphene with and without the nanoantennas. The spectra are normalized to achieve equal 2D peak amplitudes.

Figure 1. The variation of the enhancement factor and its linewidth, with the nanoantennas resonant frequency, is used to study the similarities and differences between resonant pump absorption and resonant Stokes emission.

A monopole nanoantenna is analogous to a transmission line (TL) resonator for SPPs at optical frequencies. The fundamental resonant mode imitates a $\lambda/2$ SPP-TL resonator and can efficiently absorb or radiate light waves. For a fixed wavelength, any deviation from the resonant length reduces the efficiency of absorption and radiation. The experiment primarily focuses on the enhancement of the G and 2D peaks. The D peak was excluded because it represents the degree of disorder and defects in the graphene crystal which could be simply enhanced as a result of graphene damage during the nanofabrication process without involving any of the aforementioned plasmonic mechanisms. Moreover, the spectral separation between the incident wavelength, G-, and 2D-peaks ensures that a given nanoantenna exclusively resonates either at the incident wavelength or only one of the Stokes wavelengths.

2 Materials and methods

As Figure 1 depicts, the devices consisted of arrays of 22 nm-thick gold rectangular nanorods patterned over a graphene monolayer grown by chemical vapor deposition, on a 285 nm-thick thermally-grown silicon-dioxide layer, on a silicon substrate. Gold lift-off with e-beam exposed bi-layer PMMA (producing a re-entrant profile) was used to define the nanoantennas. Each array spans a 20 μm-by-20 μm area and contains 40-by-40 nanoantennas uniformly distributed with a pitch size of 500 nm along both directions. The lengths of the nanoantennas for different arrays varied from 50 to 170 nm for two widths of 40 nm and 55 nm. Unlike most relevant works where graphene is transferred after patterning the nanostructures (an approach that significantly degrades the quality of graphene due to tears, folds, and wrinkles), the nanoantennas used in this work have been fabricated directly on graphene whose quality has been well-preserved as is evident from a small increase in the D-peak amplitude after the fabrication process (Figure 1D). The measurement was carried out by a confocal Raman microscope (WITec Alpha 300R) where a 1 μm laser spot (50× objective) at a wavelength of 633 nm was raster-scanned with 50 nm steps over the samples and Raman spectra were recorded at each pixel. For large-area surface-enhanced Raman spectroscopy (SERS) applications, where even larger arrays are required, laser interference lithography (LIL) may be used for patterning the plasmonic nanostructures [26, 27].

3 Results and discussion

Figure 2A displays the image associated with the G peak amplitude covering the arrays of 55 nm-wide nanoantennas with lengths ranging from 58 nm to 118 nm. For very short nanoantennas, the contrast between the unpatterned graphene background and the patterned area is insignificant. Thereby, these nanoantennas do not strongly interact with any of the wavelengths involved in the experiment. However, as the nanoantennas length increases, the contrast between the background and the areas covered by nanoantennas becomes more evident, clearly exhibiting enhancement of the G amplitude in graphene. The enhancement monotonically increases with nanoantenna length ℓ until a maximum is reached at ℓ=83 nm. Beyond the maximum, any further increase in length monotonically reduces the enhancement until it completely vanishes for very long nanoantennas. A similar trend is observed for the 2D peak (Figure 2B) but the maximum enhancement is reached for ℓ=108 nm. Figure 2D–F depict the linear profile of the Raman images 2A to 2C, respectively, taken across the middle of the nanoantennas arrays.

The fact that the Raman amplitudes at the G and 2D peaks maximize for the nanoantennas of different lengths, and consequently of different resonance wavelengths, suggests that the underlying enhancement mechanism relies on the resonant coupling of the G-line ($\lambda\approx$703 nm) and 2D-line ($\lambda\approx$763 nm) to the nanoantennas with ℓ=83 nm and ℓ=108 nm, respectively. Conversely, the local field enhancement mechanism at the pump wavelength should have resulted in maximum enhancement for the peaks at a common ℓ. More insight into the mechanism of the observed enhancement may be gained by examining the Raman peaks originating from the underlying silicon substrate. It has been previously shown that the transmittance of monopole nanoantennas exhibits a deep reduction at the resonant wavelength [28]. Therefore, Raman enhancement due to the resonant absorption at the pump wavelength should be accompanied by a sharp drop in the transmitted power through the nanoantenna arrays and consequently a dramatic decline in the photon flux reaching the silicon substrate. Since the depth of focus of the objective lens in the measuring apparatus is of the order of several microns and the silicon substrate is <300 nm below the graphene layer, the measurement can easily probe the Raman signals in the silicon as well. A sharp drop in the amplitude of the silicon's Raman emission coinciding with the maxima of the graphene Raman lines would indicate resonant absorption by the nanoantennas, thus, providing evidence of Raman enhancement through

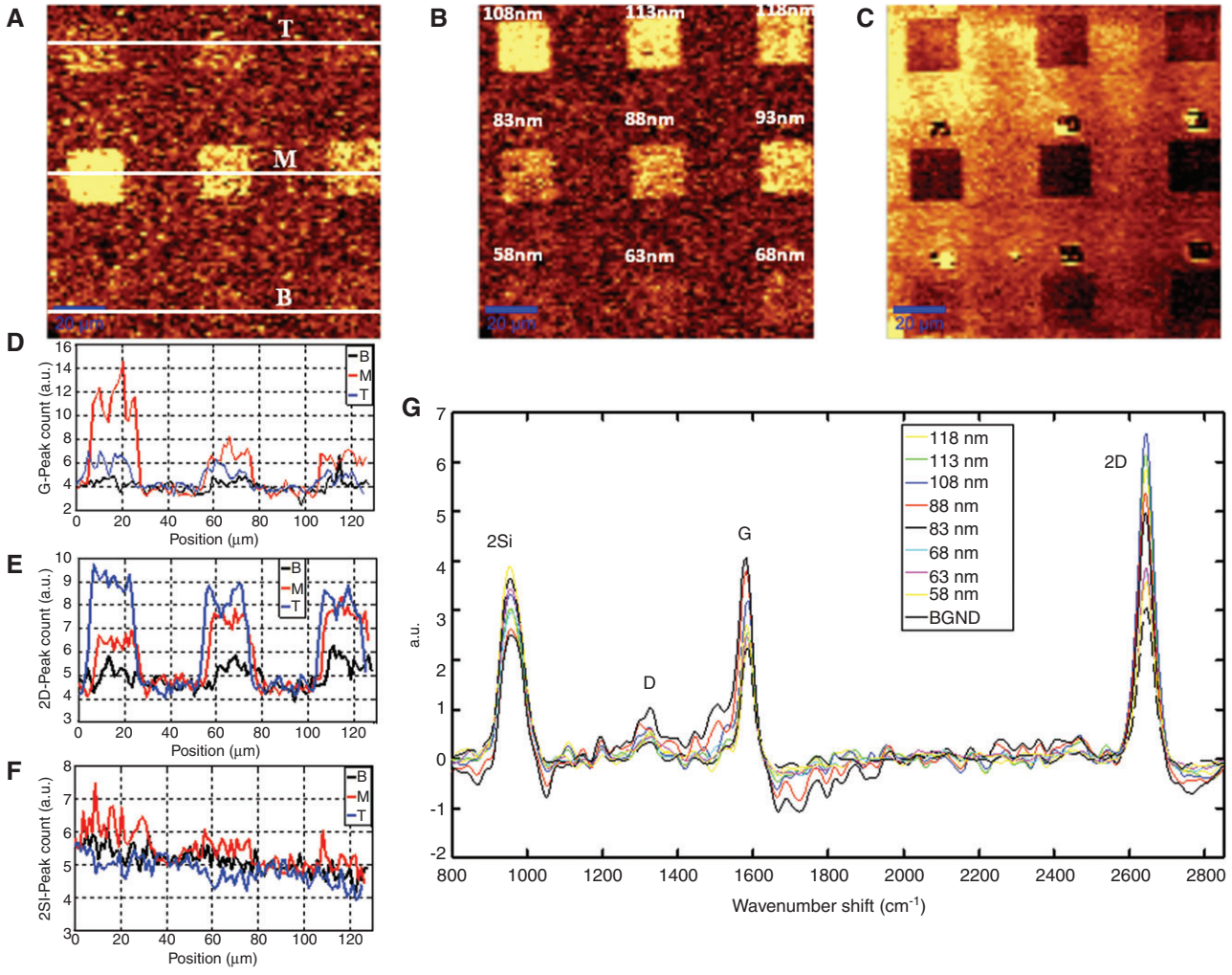

Figure 2 Raman images associated with the amplitude of (A) G peak, (B) 2D peak, and (C) 2Si peak. The nanoantenna lengths are indicated on the 2D peak image. (D–F) The line cuts of the images of part (A), (B), and (C) through the middle of the arrays. (G) Average Raman spectra over nanoantenna arrays at different lengths.

the local field enhancement at the pump wavelength, i.e., the first mechanism. Conversely, an approximately constant silicon Raman amplitude would advocate the second Raman enhancement mechanism involving resonant emission at the Stokes wavelengths.

Aside from the familiar 520 cm^{-1} line due to Si-Si bonds (Si-peak), there is also a higher order silicon peak around 970 cm^{-1} (2Si-peak) which could be used for this study. In the measurement both Si and 2Si peaks have been simultaneously observed along with the G and 2D peaks of graphene. Figure 2C illustrates the corresponding Raman image for the 2Si peak and Figure 2G shows the whole Raman spectrum at different nanoantenna lengths. The 2Si peak is presented here since it is closer to the graphene lines. Otherwise, qualitatively similar results have been obtained from the Si peak. As shown in Figure 2C, although there is a reduction in the amplitude of the 2Si peak where nanoantenna arrays are located, it does not vary much among nanoantennas at different lengths. Hence, the experimental observations are consistent with an enhancement mechanism based on nanoantennas resonant coupling to the Stokes photons.

Similar results have been also achieved using narrower rectangular monopole nanoantennas with a width of 40 nm, where this time the amplitude of the G and 2D peaks reach a maximum for nanoantennas with ℓ=78 nm and 93 nm, respectively, and the 2Si amplitude is again almost flat. This observation is consistent with the previous results showing that decreasing the width of a monopole nanoantenna red-shifts its resonant wavelength [28]. Therefore, to resonate at a given wavelength narrower nanoantennas must be shorter.

In order to quantitatively model the experimental results, the electromagnetic performance of the

nanoantennas were numerically analyzed by means of the transmission line (TL) model developed by Mousavi et al. [28] as well as a more rigorous full-wave three-dimensional finite-element method (FEM) analysis. Based on the TL model, an SPP round-trip along the nanoantenna at the resonance wavelength should amount to a phase shift equal to an integral multiple of 2π (Figure 3A). The phase shift due to the propagation of the SPP mode excited on the TL may be found from the effective propagation constant n_{eff} for an infinitely long waveguide with the same cross-section as the nanoantennas (Figure 3B) and the phase retardation from the reflections at the two ends may be estimated through the spatial extent of the fringing fields in the two-dimensional mode profile. Therefore, the resonance condition results in $\lambda_m = m(2\ell_{eff} n_{eff})$, where λ_m indicates the resonant wavelength of the mth order mode and ℓ_{eff} represents the effective length of the TL, which is the sum of its physical length ℓ and the length of the fringing fields at the two ends. Figure 3B shows n_{eff} as a function of λ and the dashed-line curves in Figure 3E depict the resulting resonant wavelengths for the two widths used in the experiments.

Figure 3C–D illustrate the electric and magnetic field profiles obtained from FEM for a representative 105 nm-long nanoantenna at the resonance wavelength in the plane tangent to the bottom facet of the nanoantenna coinciding with the plane of the graphene film. These profiles demonstrate a typical dipolar field distribution with small mode areas and strong electric field magnitudes at the ends and corners, all of which are generic to this kind of nanoantenna at optical frequencies [28]. The solid lines in Figure 3E show the resonance wavelengths of the nanoantennas as a function of lengths derived from the FEM analysis. The results of the TL and FEM models are in good agreement and clearly indicate that the lengths at which the measured amplitudes of the G and 2D peaks

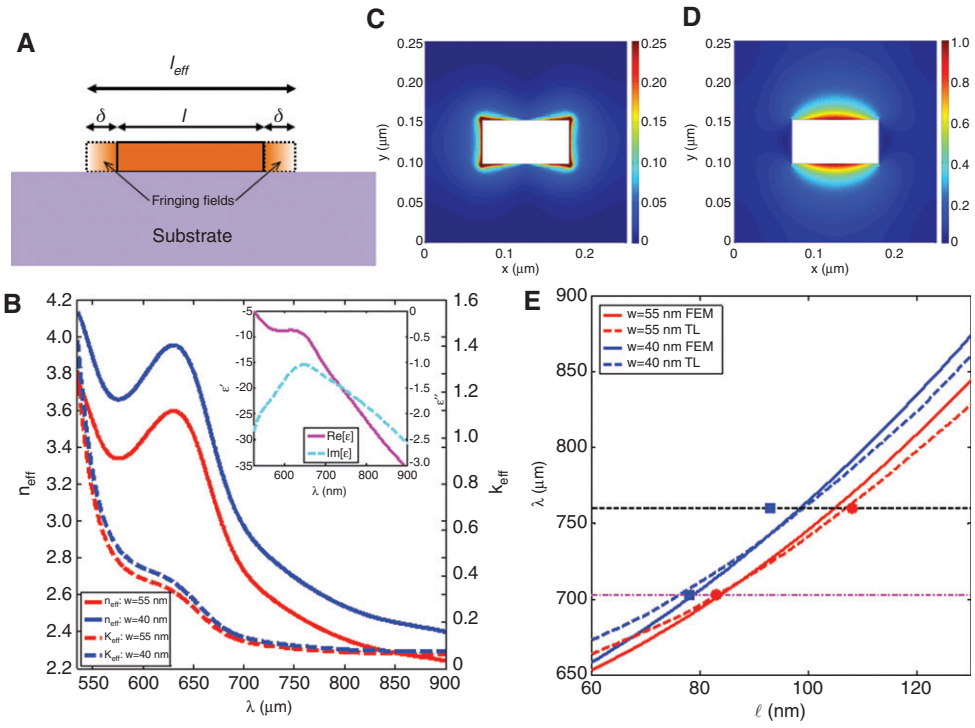

Figure 3 (A) Schematic of a monopole optical nanoantenna as a SPP transmission line resonator. ℓ signifies the physical length and δ_{eff} represents the extension of the evanescent fringing fields beyond the ends. (B) Dispersion of the effective index (solid lines) and extinction coefficient (dashed lines) for the fundamental mode of an infinitely long gold waveguide associated with the 55 nm-wide (red) and 40 nm-wide (blue) nanoantennas. The inset depicts the real and imaginary parts of the gold dielectric function in the spectral region of interest. (C–D) The profiles of, respectively, |E| and |H| for an individual 105 nm-long nanoantenna in the plane of the substrate at its resonance wavelength of 763 nm. The profiles are normalized to possess unity maxima. White rectangles represent the physical extent of the nanoantenna. (E) The resonance wavelength as a function of the physical length for the nanoantennas with w=55 nm (red) and 40 nm (blue) computed by the full-wave finite-element method (FEM) (solid lines) and the TL model (dashed lines). The horizontal magenta and black dashed lines illustrate the wavelengths of the G and 2D Raman peaks in graphene for an incident wavelength of 633 nm. The red circles and blue squares designate the nanoantenna lengths for which the maxima of the Raman peaks were experimentally observed for w=55 nm and 40 nm, respectively. The inset shows the resonance quality factor as a function of length.

maximize, as represented by the squares and circles in Figure 3E, coincide with the resonance at the G and 2D wavelengths, respectively. Therefore, the observed Raman enhancement is undoubtedly due to the nanoantennas resonant coupling to the red-shifted Stokes, rather than the pumping photons.

Figure 4A–B show the experimental G and 2D peak Raman enhancement factors as a function of ℓ for the two nanoantenna sets of different widths, respectively. The enhancement factor for a specific nanoantenna array ε is defined as the ratio of the average Raman amplitude measured over the array to the same quantity over the neighboring unpatterned graphene area. The figures clearly demonstrate that the peak enhancement factors for the G and 2D peaks occur for the nanoantennas whose resonant wavelengths coincide with the G and 2D Stokes wavelengths, respectively. In addition, the maximum enhancement factors for the two Raman peaks differ considerably from each other by more than a factor of 2. Moreover, the dramatic difference in the enhancement spectral widths for the G and 2D peaks is a manifestation of the dispersive nature of the underlying enhancement mechanism. All of these experimental observations are inconsistent with the resonant pump absorption, which is the underlying mechanism to predict almost equal enhancement factors and spectral widths at a common ℓ. These results suggest that ascribing the Raman scattering enhancement in graphene solely to the SPP-mediated resonant pump absorption when the measured enhancement factors for the G and 2D peaks differ considerably, as is prevalent in the literature, is at least controversial, if not erroneous.

To demonstrate a situation where the resonant pump absorption produces Raman enhancement, nanoantennas resonant with the incident wavelength of 633 nm are required. As Figure 3D shows, such nanoantennas should be much smaller than the monopole nanoantennas used in this work. In addition, gold's interband transition loss becomes significant at this wavelength and hinders a direct and clear demonstration, merely because the resonances of such small gold structures have low quality factors and will be too broad to resolve the spectral separations among the Stokes wavelengths. In fact, such broad resonance in self-assembled nanoparticles or a combination of fabrication defects and irregular geometries in patterned nanostructures

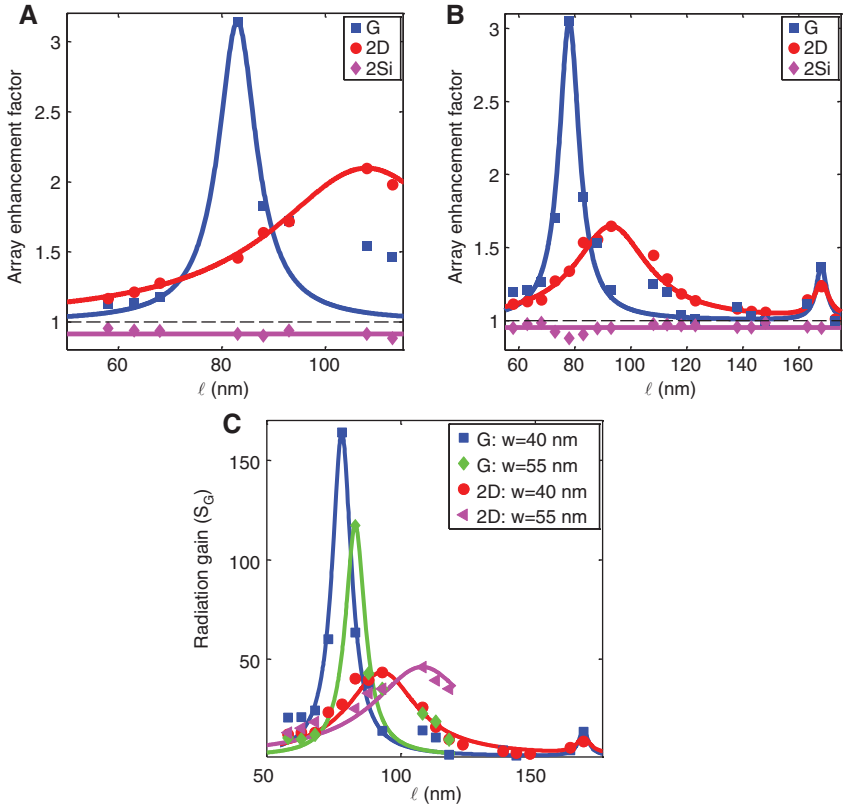

Figure 4 Experimental enhancement factors ε as a function of nanoantenna lengths for w=55 nm (A) and 40 nm (B). The solid lines are Lorentzian line-shape fits to the experimental data. (C) Scattering cross-section enhancement factor for an individual nanoantenna S_G as a function of the lengths extracted from (A) and (B).

might have been an important reason for the lack of discretion between the two mechanisms in graphene.

Alternatively, utilizing higher-order resonant modes of nanoantennas relieves these issues. For instance, the second- and third-order longitudinal resonant modes correspond to λ and $3\lambda/2$ resonators, respectively. This technique allows longer nanoantennas to resonate at the pump wavelength, but at the cost of a larger mode volume. Together with the higher loss of gold at shorter wavelengths, it reduces the achievable Raman enhancement factor. Compared to the fundamental mode, higher-order modes of plasmonic resonators are generally underutilized and rarely considered as a viable means for nanophotonics. This is partly because many of them may not be directly excited by plane waves due to their anti-symmetric mode profile. The second-order mode of a monopole nanoantenna, i.e., the λ SPP-TL resonator, falls in this category. The third-order mode, however, maintains a symmetric mode profile which can be excited by plane waves. Figure 4B clearly shows the contribution of this mode to the graphene Raman enhancement as two coincident peaks in the enhancement factor of the G and 2D peaks at ℓ=168 nm. Unlike the enhancement factor peaks originating from the resonance at the Stokes wavelengths for shorter nanoantennas, these have almost equal widths and amplitudes, which is consistent with the incident field enhancement mechanism at the pump wavelength. The relatively lower enhancement factor is expected due to the lower quality factor and larger mode volume of the higher-order resonance.

It has become customary in the literature to report the ratio of the maximum measured amplitude of the Raman peaks in graphene near the plasmonic nanostructure to that at a reference point, often the bare substrate, as the figure of merit of the plasmonic enhancement. Such quantification relies on the best observed performance and is sample dependent. More fundamentally, it is well-known that the electromagnetic fields diverge at sharp (subwavelength) corners even in non-resonant scatterers [29, 30]. Therefore, such quantifications are inaccurate since local geometric irregularities, which are often random and unintended, due to material and fabrication defects, significantly contribute to the so-called enhancement factor. Moreover, the overall size of the nanostructure does not directly factor in such figures of merit. It is obvious that many applications of plasmonic enhancement require an array of nanostructures. Thus, the geometric extent of the unit cell should be considered when defining the figure of merit. Given that plasmonic nanoantennas are essentially antennas, the figure of merit of the plasmonic enhancement, or equivalently the scattering gain, S_G could be defined as the ratio of the effective scattering cross-section A_{eff} to the geometric cross-section A_g:

$$S_G = \frac{A_{eff}}{A_g} \tag{1}$$

Theoretical evaluation of S_G involves solving a standard electromagnetic scattering problem. Its experimental determination for an array of nanoantennas is also straightforward as follows. Let P_0 and P_1 denote the average emitted Raman powers from one of the Stokes processes, from an unpatterned uniform area of graphene as large as the unit cell of the nanoantenna array A_0 and from a unit cell of the nanoantenna array, respectively. The array enhancement factor defined above and depicted in Figure 4A–B is, thus, equal to $\varepsilon = \frac{P_1}{P_0}$. Given that the enhancement factor of an unpatterned unit cell by definition equals to 1, and ignoring the area that is blocked by the geometric area of a nanoantenna A_g from the incident field ($A_g << A_0$), then $\varepsilon - 1$ is the contribution of an individual nanoantenna to the enhancement of the Raman scattering amplitude. Thus, the effective scattering-cross section of a single nanoantenna reads $A_{eff} = (\varepsilon - 1)A_0$. This is substituted in equation (1) in order to experimentally extract the scattering cross-section gain of a single nanoantenna. Figure 4C gives S_G as a function of ℓ for the G and 2D peaks of the two nanoantenna sets at different widths, where it is evident that scattering cross-section gains as high as 160 may be attained for a single nanoantenna. The measured arrays are sparsely populated with nanoantennas, ranging from <1% geometric fill factor for ℓ=50 nm to 3.7% for ℓ=170 nm. Since the mode volume of a single nanoantenna is small, as shown by Figure 3C–D, the arrays could be much more densely filled with nanoantennas in order to obtain even higher array enhancement factors. From a practical point of view, the mechanism of Raman enhancement based on tuning nanoantennas to the Stokes wavelengths has the advantage that one could selectively choose which Raman process in graphene to enhance, whereas the resonant pump absorption mechanism inevitably enhances all the Raman processes almost equally.

4 Conclusions

In conclusion, the enhancement of Raman scattering in graphene was demonstrated exclusively based on resonant Stokes emission by monopole gold nanoantennas. This case was experimentally compared to the similar effect caused exclusively by resonant pump absorption using the third-order longitudinal SPP mode of the

monopole nanoantennas. Both mechanisms exhibited a large enhancement in the scattering cross-section, up to 160 for resonant Stokes emission and as high as 20 for resonant pump absorption. With such high gains in the scattering cross-section and their small geometric size, nanoantenna arrays provide a viable means for ultrasensitive and efficient surface-enhanced Raman spectroscopy as well as other nonlinear optical processes in graphene.

It was also demonstrated that these mechanisms affect graphene G and 2D Raman scattering quite differently. It was shown that the resonant pump absorption symmetrically enhances both the G and 2D peaks with an equal factor and the enhancement maintains the same spectral width for both processes. On the other hand, it was found that the resonant Stokes emission mechanism asymmetrically enhances the two processes with substantially different enhancement factors and spectral linewidths. The difference was explained based on the underlying physics for each mechanism. The resonant pump absorption is common to both G and 2D processes, enhancing the local incident field, and consequently the scattering cross-section for both equally, whereas the resonant Stokes emission favors only that Stokes process being tuned, resulting in quite different enhancement factors and spectral linewidths for the G and 2D peaks. These results shed light on existing ambiguities and misinterpretations on the mechanisms of plasmonic Raman enhancement by optical nanostructures in graphene, and provide experimental benchmarks for their identification. In particular, those configurations reporting significant mismatch between the G and 2D peak enhancement factors must be inevitably involved in the resonant Stokes emission to some degrees, if not as the main mechanism. Simultaneous contribution of both mechanisms may be justified in deep sub-wavelength nanostructures due to their low quality factors and broad SPP resonances. Moreover, this work introduced a new figure of merit for quantifying the overall merit of plasmonic nanostructures in enhancing nonlinear optical processes, including Raman scattering, in terms of the scattering-cross section gain and discussed a method for its experimental determination. This new enhancement figure of merit is fundamentally more accurate, practically more useful, and universally more robust and reproducible against sample dependencies than the common practice definition in terms of the highest observed Raman amplitude at isolated hot spots in the vicinity of plasmonic nanostructures.

Acknowledgments: The work of B. G. G., F. V., and P. B. is, in part, supported by the Natural Sciences and Engineering Research Council of Canada. F.V. acknowledges financial support from the Canada Foundation for Innovation (CFI) and the Ontario Ministry of Research and Innovation (MRI) through the Leaders of Opportunity (LOF) fund.

References

[1] Bonaccorso F, Sun Z, Hasan T, Ferrari AC. Graphene photonics and optoelectronics. Nat Photon 2010;4:611–22.
[2] Grigorenko AN, Polini M, Novoselov KS. Graphene plasmonics. Nat Photon 2012;6:749–58.
[3] Gan X, Shiue R-J, Gao Y, Mak KF, Yao X, Li L, Szep A, Walker D, Hone J, Heinz TF, Englund D. High-contrast electrooptic modulation of a photonic crystal nanocavity by electrical gating of graphene. Nano Lett 2013;13:693–6.
[4] Fang Z, Liu Z, Wang Y, Ajayan PM, Nordlander P, Halas NJ. Graphene-antenna sandwich photodetector. Nano Lett 2012;12:3808–13.
[5] Yao Y, Kats MA, Genevet P, Yu N, Song Y, Kong J, Capasso F. Broad electrical tuning of graphene-loaded plasmonic antennas. Nano Lett 2013;13:1257–64.
[6] Emani NK, Chung TF, Ni XJ, Kildishev AV, Chen YP, Boltasseva A. Electrically tunable damping of plasmonic resonances with graphene. Nano Lett 2012;12:5202–6.
[7] Kim J, Son H, Cho DJ, Geng BS, Regan W, Shi SF, Kim K, Zettl A, Shen YR, Wang F. Electrical control of optical plasmon resonance with graphene. Nano Lett 2012;12:5598–602.
[8] Yariv A. Quantum electronics. 3rd Ed. New York: Wiley, 1989.
[9] Purcell EM. Spontaneous emission probabilities at radio frequencies. Phys Rev 1946;69:681.
[10] Scully MO, Zubairy MS. Quantum optics. Cambridge: Cambridge University Press, 1997.
[11] Maier SA. Plasmonic field enhancement and SERS in the effective mode volume picture. Opt Express 2006;14:1957–64.
[12] Iwase H, Englund D, Vuckovic J. Analysis of the purcell effect in photonic and plasmonic crystals with losses. Opt Express 2010;18:16546–60.
[13] Ferrari AC, Meyer JC, Scardaci V, Casiraghi C, Lazzeri M, Mauri F, Piscanec S, Jiang D, Novoselov KS, Roth S, Geim AK. Raman spectrum of graphene and graphene layers. Phys Rev Lett 2006;97:187401.
[14] Dresselhaus MS, Jorio A, Hofmann M, Dresselhaus G, Saito R. Perspectives on carbon nanotubes and graphene Raman spectroscopy. Nano Lett 2010;10:751–8.
[15] Das A, Pisana S, Chakraborty B, Piscanec S, Saha SK, Waghmare UV, Novoselov KS, Krishnamurthy HR, Geim AK, Ferrari AC, Soodi AK. Monitoring dopants by Raman scattering in an electrochemically top-gated graphene transisto. Nature Nanotechnology 2008;3:210–4.
[16] Heeg S, Fernandez-Garcia R, Oikonomou A, Schedin F, Narula R, Maier SA, Vijayaraghavan A, Reich S. Polarized plasmonic enhancement by Au nanostructures probed through Raman scattering of suspended graphene. Nano Lett 2013;13:301–8.
[17] Hao Q, Wang B, Bossard JA, Kiraly B, Zeng Y, Chiang I-K, Jensen L, Werner DH, Huang TJ. Surface-enhanced Raman scattering study on graphene-coated metallic nanostructure substrates. J Phys Chem C 2012;116:7249–54.

[18] Grande M, Stomeo T, Bianco GV, Vincenti MA, de Ceglia D, Petruzzelli V, Bruno G, De Vittorio M, Scalora M, D'Orazio A. Fabrication of doubly resonant plasmonic nanopatch arrays on graphene. Appl Phys Rev 2013;102:231111.
[19] Khorasaninejad M, Raeis-Zadeh SM, Jafarlou S, Wesolowski MJ, Daley CR, Flannery JB, Forrest J, Safavi-Naeini S, Saini SS. Highly enhanced Raman scattering of graphene using plasmonic nano-structure. Scientific Reports 2013;3:2936.
[20] Xu W, Xiao J, Chen Y, Chen Y, Ling X, Zhang J. Graphene-veiled gold substrate for surface-enhanced Raman spectroscopy. Adv Mater 2013;25:928–33.
[21] Sarau G, Lahiri B, Banzer P, Gupta P, Bhattacharya A, Vollmer F, Christiansen S. Enhanced Raman scattering of graphene using arrays of split ring resonators. Adv Opt Mat 2013;1:151–7.
[22] Kravets VG, Schedin F, Jalil R, Britnell L, Novoselov KS, Grigorenko AN. Surface hydrogenation and optics of a graphene sheet transferred onto a plasmonic nanoarray. J Phys Chem C 2012;116:3882–7.
[23] Urich A, Pospischil A, Furchi MM, Dietze D, Unterrainer K, Mueller T. Silver nanoisland enhanced Raman interaction in 805 graphene. Appl Phys Lett 2012;101:153113–4.
[24] Cheng C-E, Lin C-Y, Chang H-Y, Huang C-H, Lin H-Y, Chen C-H, Hsu C-C, Chang C-S, Chien FSS. Surface-enhanced Raman scattering of graphene with photo-assisted-synthesized gold nanoparticles. Optics Express 2013;21:6547–54.
[25] Hao Q, Morton SM, Wang B, Zhao Y, Jensen L, Huang TJ. Tuning surface-enhanced Raman scattering from graphene substrates using the electric field effect and chemical doping. Appl Phys Lett 2013;102:011102.
[26] Yang J, Luo F, Kao TS, Li X, Ho WG, Teng J, Luo X, Hong M. Design and fabrication of broadband ultralow reflectivity black Si surfaces by laser micro/nanoprocessing. Light: Science and Applications 2014;3:e185.
[27] Xu L, Luo FF, Tan LS, Luo XG, Hong MH. Hybrid plasmonic structures: design and fabrication by laser means. IEEE J Select Topics Quant Elect 2013;19:4600309.
[28] Mousavi SS, Berini P, McNamara D. Periodic plasmonic nano-antennas in a piecewise homogeneous background. Optics Express 2012;20:18044–65.
[29] Disfani MR, Abrishamian MS, Berini P. Electromagnetic fields near plasmonic wedges. Opt Lett 2012;37:1667–9.
[30] Jackson JD. Classical electrodynamics. 3rd Ed. New York: John Wiley, 1999.

Graphical abstract

Behnood G. Ghamsari, Anthony Olivieri, Fabio Variola, and Pierre Berini

Enhanced Raman Scattering in Graphene by Plasmonic Resonant Stokes Emission

DOI 10.1515/nanoph-2014-0014
Nanophotonics 2014; x(x): xxx–xxx

Research article: This work demonstrates Raman scattering enhancement in graphene based on plasmonic resonant enhancement of the Stokes emission, and compares this mechanism with the conventional Raman enhancement by resonant pump absorption.

Keywords: Optical nanoantennas; graphene; plasmonics; Raman scattering.